Electrochemical and Solid-State Letters, **13** (7) A88-A90 (2010)
1099-0062/2010/13(7)/A88/3/$28.00 © The Electrochemical Society

Electron Diffraction Studies of $LiNi_{1/3}Mn_{1/3}Co_{1/3}O_2$ After Charge–Discharge Cycling

H. Gabrisch[a,*,z] **and R. Yazami**[b,*]

[a]*Advanced Materials Research Institute, University of New Orleans, New Orleans, Louisiana 70148, USA*
[b]*California Institute of Technology, Pasadena, California 91125, USA*

The performance of $LiNi_{1/3}Mn_{1/3}Co_{1/3}O_2$ depends largely on the distribution of transition-metal (TM) ions over the available lattice sites within the layered rocksalt structure. Despite predictions that the TM ions take on an ordered arrangement described by a $\sqrt{3} \times \sqrt{3}R30°$ supercell, little experimental evidence is available to confirm this model. However, the observed cation distribution likely depends on synthesis conditions. Here, we present a study of commercially produced $LiNi_{1/3}Mn_{1/3}Co_{1/3}O_2$ synthesized at 1000°C before and after charge–discharge cycling. Electron diffraction shows that in-plane ordering is observed to small extents. After charge–discharge cycling, a transformation toward the cubic spinel structure and significant morphology changes are observed.
 [DOI: 10.1149/1.3424884]

Manuscript submitted December 23, 2009; revised manuscript received April 8, 2010. Published May 10, 2010.

Over the past few years, the ternary transition-metal (TM) oxide $LiNi_{1/3}Mn_{1/3}Co_{1/3}O_2$ has developed into a strong candidate for applications in high power rechargeable Li-ion batteries due to its superior thermal stability and reversible capacity compared to its $LiCoO_2$ counterpart.[1-3] $LiNi_{1/3}Mn_{1/3}Co_{1/3}O_2$ adopts the typical α-$NaFeO_2$ structure that is known of layered $LiCoO_2$ and $LiNiO_2$ and is described by the $R\bar{3}m$ space group (space group 166). In $LiCoO_2$, this structure is often called the "O3" phase, referring to the octahedral coordination of Co ions and the number of O–Co–O slabs per unit cell. The crystal structure consists of a cubic close-packed oxygen lattice (Wyckoff position 6*a*) with alternating layers of octahedral interstitial sites occupied by Li (Wyckoff position 3*b*) and TM (TM = Ni, Mn, Co, Wyckoff position 3*a*). In the coordination polyhedra description, the structure can be considered as sheets formed by edge sharing TMO_6 octahedra separated by layers of lithium ions in interstitial octahedral sites.[4] TM ions play a significant role toward the stability and electrochemical activity in this compound. Nickel is believed to be the electrochemical active species, whereas manganese provides structural stability, and cobalt supports the ordering of lithium and nickel ions onto their respective lattice sites.[5] The occupation of the 3*a* lattice site in the $R\bar{3}m$ structure with three different TM species gives rise to different cation ordering schemes, which is likely to affect the electrochemical activity and structural stability of the compound. The well-known tendency of Ni ions to exchange sites with Li ions in their respective layers introduces a local disorder that impairs electrochemical performance.[6] It has also been associated with the formation of a cubic spinel phase ($Fd\bar{3}m$ symmetry), where Li and TM ions occupy sites in the same interstitial layer.[7] First-principle calculations indicate that in-plane ordered $LiNi_{1/3}Mn_{1/3}Co_{1/3}O_2$ where Ni, Co, and Mn ions are assigned element specific lattice sites in a $\sqrt{3} \times \sqrt{3}R30°$ in-plane unit cell (Wood's notation) should be stable.[8] The available experimental results are not conclusive on a favored cation arrangement and its evolution with charge–discharge cycling or aging. For example, experimental evidence for in-plane ordering has been reported in electron diffraction studies by Yabuuchi et al. and by Zeng.[9,10] For comparison, neutron diffraction and anomalous X-ray powder diffraction data show random distribution of Mn, Ni, and Co over 3*a* sites in the $R\bar{3}m$ structure.[11]

Previously, we investigated commercial $LiNi_{1/3}Mn_{1/3}Co_{1/3}O_2$ by electron diffraction before and after long-term aging. We identified substantial variations in cation ordering in the pristine material and found indications for growth processes resulting from cation rearrangement after aging.[12] Inhomogeneous cation distribution in the pristine material converted to a mixture of O3 and spinel phases after aging or charge to high voltage. In the present study, we investigate commercial $LiNi_{1/3}Mn_{1/3}Co_{1/3}O_2$ (ENAX Inc., generation 2) in the pristine state and after cycling.

Experimental

Commercial $LiNi_{1/3}Mn_{1/3}Co_{1/3}O_2$ and cycled cathodes prepared of the powder were obtained from ENAX, Inc. (generation 2, powder prepared according to the method published in Ref. 9). The cathodes underwent 520 charge–discharge cycles between 3.0 and 4.3 V and were stopped in the discharged state. The capacity loss measured after cycling was 15%.

The cycled cathodes were disassembled and the active material was retrieved from the cathodes for transmission electron microscopy (TEM) specimen preparation. TEM specimens of the virgin material were prepared of the powder. Electron diffraction and dark-field imaging were performed with the JEOL 2010 transmission electron microscope at the University of New Orleans operated at 200 kV. The relative concentrations of Mn, Ni, and Co were determined in some particles by energy-dispersive spectroscopy. Experimental diffraction patterns were compared to patterns simulated with the software Desktop Microscopist using unit cells published in the literature; a list can be found in Ref. 12.

Results and Discussion

Compared to the generation 1 material supplied by the same company, the generation 2 compound has a more homogeneous crystal structure.[12] The majority of particles in the investigated $LiNi_{1/3}Mn_{1/3}CoO_2$ (ENAX, generation 2) are completely indexed as an O3 phase, indicating a random distribution of TM ions (22 out of 31 or 71%). Of the remaining particles, three show typical diffractions of the $\sqrt{3} \times \sqrt{3}R30°$ unit cell plane ordering, whereas five particles have spinel type diffraction patterns. A summary of the cation ordering observed in the analyzed particles is given in Table I.

Although most particles are single crystalline, ~20% of the analyzed particles in the pristine material are polycrystals. In most cases, the polycrystalline particles consist of two crystals indexed as an O3 phase that are related by a twin boundary (4 out of 5). An example is shown in Fig. 1, where diffraction patterns of each crystal (Fig. 1c and d) are shown together with the pattern obtained from the whole particle (Fig. 1b). The pattern in Fig. 1b is a superposition of the patterns shown in Fig. 1c and d. The image in Fig. 1a is taken in the dark-field condition using the $(\bar{1}01\bar{1})$ reflection of the diffraction pattern shown in Fig. 1d that corresponds to the bright, larger crystal in Fig. 1a.

During cycling, the amount of polycrystals and the fraction of particles with a long-range order remain approximately constant. A significant change is observed in the amount of spinel phase that

* Electrochemical Society Active Member.
z E-mail: heike.gabrisch@gkss.de

Table I. Analysis of commercial $LiNi_{1/3}Mn_{1/3}Co_{1/3}O_2$: The numbers reflect the count of diffraction patterns in each category. Some particles were polycrystals, the total number of analyzed patterns is given in brackets at the top of each column. Twenty-five pristine particles and 15 cycled particles were analyzed.

Classification	Pristine (31)	Cycled (17)
O3	22	6
Spinel	5	8
$\sqrt{3} \times \sqrt{3}R30°$	3	2
Other	1	1

increases at the expense of the O3 phase from 16% before cycling to 47% after cycling. Energy-dispersive analysis shows only small variations in the ratio of Mn:Co:Ni. In all analyzed spectra, including those representative of the spinel phase, the values for Mn, Co, and Ni were within the ranges Mn: 0.29–0.35, Co: 0.28–0.35, and Ni: 0.32–0.36.

The intensity of spinel reflections in the pristine and cycled materials spans a wide range. A comparison is shown in Fig. 2, where the typical spinel reflections are barely visible in Fig. 2a, whereas they have an intensity identical to that of the fundamental reflections in Fig. 2c. The intensity variations in the typical spinel diffractions correspond to a gradual change in the cation ordering between the two limiting phases: layered and cubic.

The most striking observation in the cycled particles is the change in morphology in some particles. An example showing several such damaged particles is given in Fig. 3. Apparently, the particles disintegrate during cycling and form a lamellar morphology consisting of 5–10 nm thick lamellas that are stacked along the [0001] direction. An example of this morphology that we call "mille-feuille" is shown in Fig. 4, together with its diffraction pattern. The diffraction pattern can be indexed as an O3 phase, but faint

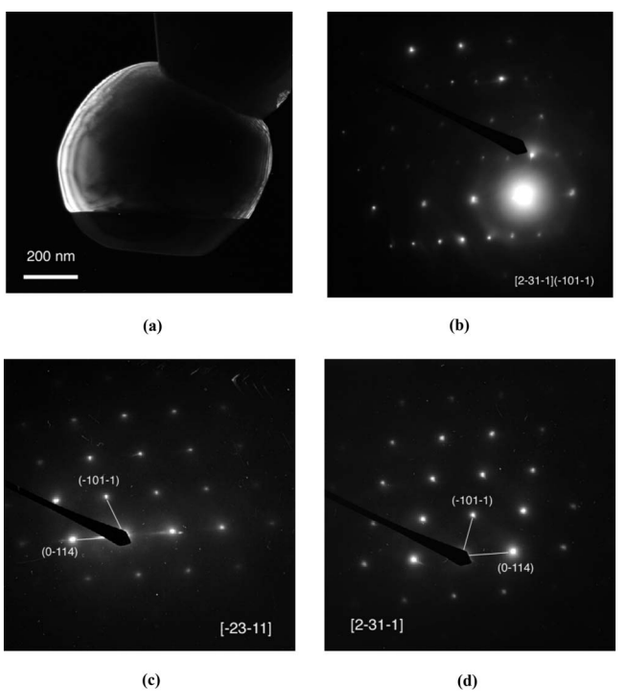

Figure 1. Image and diffraction patterns taken from a pristine, commercial polycrystalline particle. (a) Dark field image taken with a reflection unique for the bright part in the image. (b) Corresponding diffraction pattern; the reflection used for imaging is marked by the pointer. [(c) and (d)] The diffraction patterns of the two crystals.

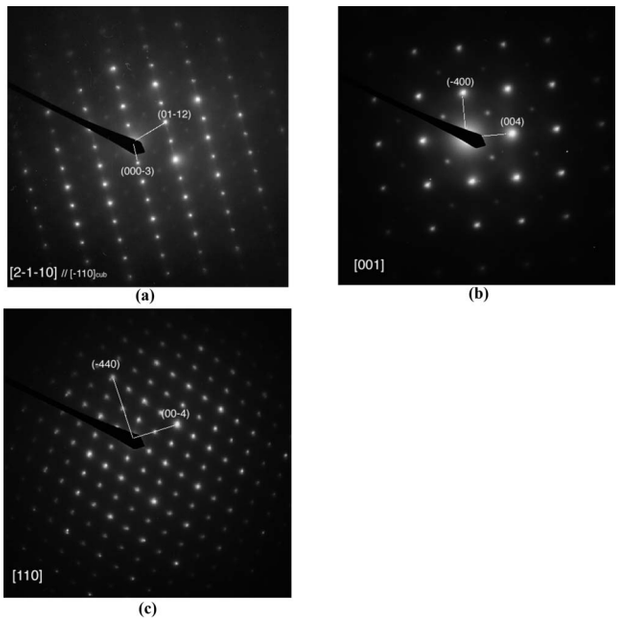

Figure 2. Electron diffraction patterns showing spinel reflections of increasing intensity from (a) to (c) corresponding to a gradual change in cation rearrangement.

contributions of spinel and $\sqrt{3} \times \sqrt{3}R30°$ ordering are also visible. A comparison between the directions in the diffraction pattern and in the image illustrates that the lamellas are separated between (0001) planes, where bonding between adjacent layers is weak. A closer look at the corresponding diffraction pattern in Fig. 4b shows that the shape of fundamental reflections is not circular but streaked along the [0001] direction. Streaking indicates the presence of planar defects such as platelike precipitates or stacking faults oriented perpendicular to the streaking direction [here, the defects lie in the (0001) planes]. In Fig. 5, a cycled particle is shown that does not have the mille-feuille morphology but has pronounced streaking in the diffraction pattern. Therefore, it is not clear that the observed

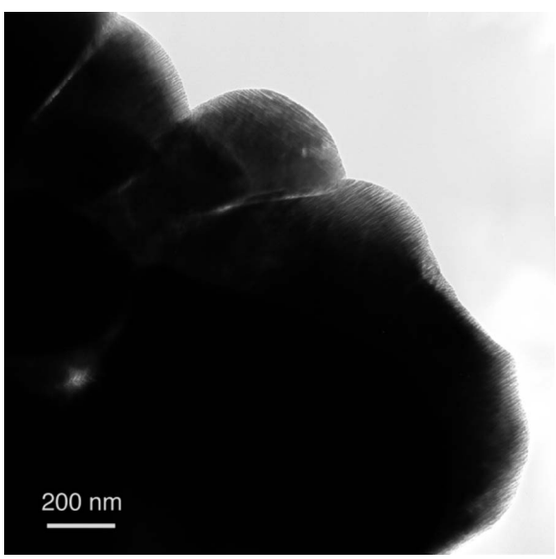

Figure 3. TEM image showing an agglomerate of $LiNi_{1/3}Mn_{1/3}Co_{1/3}O_2$ particles with a mille-feuille morphology observed after charge–discharge cycling.

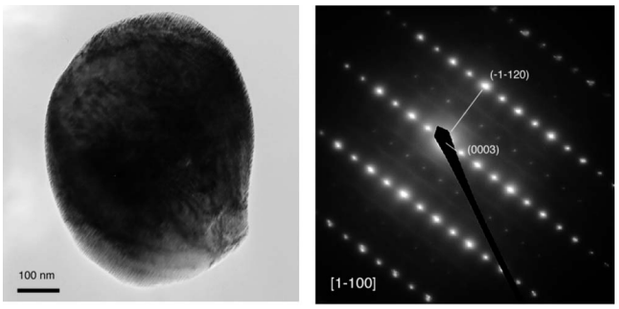

Figure 4. Image and diffraction pattern illustrating the orientation relationship between the lamella in the mille-feuille morphology and the diffraction pattern.

morphology change is responsible for the observed streaking. Possibly, stacking faults or monoatomic layers form on the {0001} planes that give rise to streaking. With continued cycling, these defects may contribute to the observed morphology change. In another study, we observed similar morphology changes in chemically delithiated $Li_xNi_{1/3}Mn_{1/3}Co_{1/3}O_2$ particles after long-time anneal, indicating that the underlying processes can take place during aging of a battery and do not require continued Li extraction and insertion (to be published). Altogether, we observed streaking in 6 out of 15 particles analyzed after cycling but only in 1 out of 22 of the pristine material.

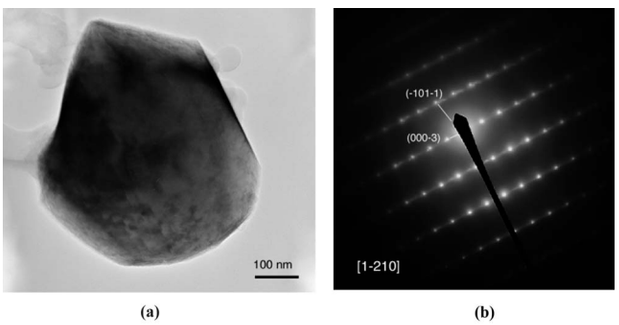

Figure 5. Image and diffraction pattern of a cycled particle. Pronounced streaking along the [0001] direction is observed in the diffraction pattern.

Conclusions

Commercial $LiNi_{1/3}Mn_{1/3}Co_{1/3}O_2$ synthesized at approximately 1000°C shows long-range ordering in about 10% of the analyzed diffraction patterns, a fraction that remains stable over charge–discharge cycling. The pristine material consists of 70% of particles with random TM ion distribution on the 3*a* lattice sites; however, after 520 charge–discharge cycles, a portion of these have transformed to spinel, so that ~47% spinel phase is observed after cycling. The mille-feuille morphology is observed frequently after cycling. Streaking in the diffraction pattern of cycled particles indicates that microscopic defects have formed on the (0001) planes.

Acknowledgment

This work was supported through the Louisiana Board of Regents, LEQSF(2007012)_ENH-PKSFI-PRS-04. We thank ENAX, Inc. of Japan for providing $LiNi_{1/3}Mn_{1/3}Co_{1/3}O_2$ powder and cycled cathodes.

References

1. T. Ohzuku and Y. Makimura, *Chem. Lett.*, **7**, 642 (2001).
2. I. Belharouak, Y. K. Sun, J. Liu, and K. Amine, *J. Power Sources*, **123**, 247 (2003).
3. J. W. Wen, H. J. Liu, H. Wu, and C. H. Chen, *J. Mater. Sci.*, **42**, 7696 (2007).
4. X. Luo, X. Wang, L. Liao, X. Wang, S. Gamboa, and P. J. Sebastian, *J. Power Sources*, **161**, 601 (2006).
5. M. S. Whittingham, *Chem. Rev. (Washington, D.C.)*, **104**, 4271 (2004).
6. T. Nedoseykina, S.-S. Kim, and Y. Nitta, *Electrochim. Acta*, **52**, 1467 (2006).
7. Y. Hinuma, Y. S. Meng, K. Kang, and G. Ceder, *Chem. Mater.*, **19**, 1790 (2007).
8. Y. Koyama, Y. Makimura, I. Tanaka, H. Adachi, and T. Ohzuku, *J. Electrochem. Soc.*, **151**, A1499 (2004).
9. N. Yabuuchi, Y. Koyama, N. Nakayama, and T. Ohzuku, *J. Electrochem. Soc.*, **152**, A1434 (2005).
10. Y. W. Zeng, *J. Power Sources*, **183**, 316 (2008).
11. P. S. Whitfield, I. J. Davidson, L. M. D. Cranswick, I. P. Swainson, and P. W. Stephens, *Solid State Ionics*, **176**, 463 (2005).
12. H. Gabrisch, T. Yi, and R. Yazami, *Electrochem. Solid-State Lett.*, **11**, A119 (2008).